Batteries & Supercaps

Research Article
doi.org/10.1002/batt.202400601

Chemistry Europe
European Chemical Societies Publishing

www.batteries-supercaps.org

Polyoxovanadates as Effective Coating Materials for Layered Ni-Rich Oxide Cathodes in Liquid- and Solid-State Batteries

Barbara Nascimento Nunes,*[a] Masooma Ibrahim,[b] Ruizhuo Zhang,[a] Wengao Zhao,[a] Ziyan Zhang,[a] Aleksandr Kondrakov,*[a, c] and Torsten Brezesinski*[a]

Advanced coatings for improving the electro-chemo-mechanical stability of high-capacity, layered Ni-rich oxide cathode materials play an important role in modern battery technology. Vanadium-based protective coatings are particularly promising owing to their ability to provide high ionic conductivity and their intrinsic robustness. In addition, diminishing or eliminating residual lithium through surface coating shows great promise in mitigating capacity loss and addressing associated challenges. Herein, we report on a strategic exploration of a facile coating approach for Ni-rich $LiNi_xCo_yMn_{1-x-y}O_2$ (NCM851005, 85% Ni content) utilizing polyoxovanadate. Specifically, $TBA_3H_3[V_{10}O_{28}]$ was applied due to its solubility in non-aqueous media, avoiding H_2O-induced side reactions and achieving a more uniform surface coverage. The cycling performance of NCM851005 before and after modification was tested in conventional Li-ion cells, as well as in all-solid-state batteries with a lithium thiophosphate superionic electrolyte. Our findings highlight the potential of polyoxovanadate-derived protective coatings for improving the cyclability of Ni-rich cathodes.

Introduction

With the widespread adoption of lithium-ion batteries (LIBs), layered oxides of type $LiNi_xCo_yMn_{1-x-y}O_2$ (NCM or NMC) have become one of the most important cathode active materials (CAMs).[1–3] Despite their better cycling performance than $LiNiO_2$ (LNO) for example,[4] electro-chemo-mechanical degradation during battery operation results in capacity fade.[5] In fact, one of the primary causes of capacity decay as well as safety concerns are due to interfacial side reactions with the electrolyte, triggering metal dissolution (corrosion), lithium consumption, and gassing. To address these issues, surface coatings are implemented as a kind of artificial cathode electrolyte interphase (CEI), providing physical separation between the CAM and the electrolyte.[6–8] However, an ideal coating should also offer a high permittivity, as the formation of CEIs introduces an additional barrier, increasing the overall cell resistance during cycling.[6] For instance, oxide coatings are commonly utilized to establish a chemically stable protective layer on NCMs. Nevertheless, a drawback to their application is a possible increase in impedance, hindering lithium diffusion and reducing specific capacity due to the introduction of redox-inactive material.[7] In light of this, vanadium oxides, in particular V_2O_5, emerge as a compelling alternative for coating applications (note that layered structures allow for facile intercalation of lithium ions).[9,10] V_2O_5-based coatings are usually of relatively low cost and can be readily prepared, offering high ionic conductivity as well as enhanced stability.[11–13] Liu and coworkers reported on improved performance of $LiNi_{1/3}Co_{1/3}Mn_{1/3}O_2$ (NCM111, 33% Ni content) upon coating with V_2O_5. The capacity retention after 100 cycles increased from 59 to 83%, which was attributed to the coating suppressing adverse side reactions and reducing charge-transfer resistance.[13] Similarly, Lv *et al.* observed an enhanced stability for V_2O_5-coated NCM111.[11] In this case, better rate performance was explained by the removal of residual lithium (surface impurities) by the V_2O_5. Indeed, other studies have reported the formation of lithium vanadates, such as LiV_3O_8[14–16] or LiV_2O_4,[17] when coating NCMs with vanadium compounds in absence of an additional lithium source. This is advantageous for removing excess lithium from the surface, given that NCMs when exposed to ambient conditions are prone to forming LiOH and carbonates.[18] Exposure to H_2O is known to be detrimental to this class of materials, particularly for Ni-rich NCMs, as it leads to H^+/Li^+ exchange and the formation of LiOH, or even nickel oxyhydroxides and rock salt-type phases upon annealing.[19,20] The latter species lead to capacity loss and challenges related to the surface during slurry preparation and casting onto the current collector.[21,22]

[a] Dr. B. Nascimento Nunes, R. Zhang, Dr. W. Zhao, Z. Zhang, Dr. A. Kondrakov, Dr. T. Brezesinski
Battery and Electrochemistry Laboratory (BELLA), Institute of Nanotechnology, Karlsruhe Institute of Technology (KIT), Kaiserstr. 12, 76131 Karlsruhe, Germany
E-mail: barbara.nunes@kit.edu
torsten.brezesinski@kit.edu
aleksandr.kondrakov@basf.com

[b] Dr. M. Ibrahim
Institute of Nanotechnology, Karlsruhe Institute of Technology (KIT), Kaiserstr. 12, 76131 Karlsruhe, Germany

[c] Dr. A. Kondrakov
BASF SE, Carl-Bosch-Str. 38, 67056 Ludwigshafen, Germany

Supporting information for this article is available on the WWW under https://doi.org/10.1002/batt.202400601

Research Article
doi.org/10.1002/batt.202400601
Chemistry Europe
European Chemical Societies Publishing

Xiong and coworkers were the first reporting vanadium oxides as coating materials for layered Ni-rich CAMs (NCM811, 80% Ni content).[15,16] The material was prepared by blending NCM811 and vanadium acetylacetonate (0.5 wt.% V_2O_5)[16] or ammonium metavanadate (1 wt.% V_2O_5)[15] in ethanol, followed by calcination at 400 and 300 °C, respectively. In both cases, the coating material was identified to be composed of V_2O_5 and LiV_3O_8. When the V_2O_5/LiV_3O_8-coated NCM811 was electrochemically tested at 60 °C, the capacity retention increased from 45% for the pristine CAM to 77% after 100 cycles.[15] Zhang *et al.* studied Li_3VO_4 coating of NCM811 by reacting the CAM with V_2O_5 and LiOH in aqueous medium, and then calcining it at 700 °C.[23] Even though the discharge capacities of the coated materials were lower in the initial cycles, the sample with 3 wt.% Li_3VO_4 achieved a capacity retention of 84% after 100 cycles, compared to only 54% for the pristine NCM811. Moreover, in several studies involving NCMs with a low nickel content, H_2O is employed as medium for mixing the CAM and vanadium compound.[11,14,23–25] Given this context, we strategically explored a facile coating method for a Ni-rich NCM, namely NCM851005 (85% Ni content), using a polyoxovanadate (POV).

Polyoxometalates (POMs) are anionic clusters characterized by a central metal atom (e.g., V^{5+}, Nb^{5+}, Mo^{6+}, Ta^{5+}, W^{6+}) surrounded by oxygen atoms and offer a wide range of sizes and shapes, being versatile building blocks capable of self-assembling into complex structures.[26–28] POMs function as electron sponges because of their intrinsic ability to reversibly absorb and release (multiple) electrons.[29] A notable feature is their solubility in different solvents depending on the counterion(s), allowing for the formation of stable and ordered films.[27] Moreover, POVs have already been employed as CAMs[30,31] and precursors to obtain other vanadium oxides, such as V_2O_5,[32] γ-LiV_2O_5,[33] $LiVO_3$, or LiV_3O_8,[34] for LIB application. However, to the best of our knowledge, no similar coating strategy has been reported in the literature. Hence, $TBA_3H_3[V_{10}O_{28}]$ (TBA: tetrabutylammonium) was selected to coat NCM851005 secondary particles, given its solubility in non-aqueous solvents, such as ethanol and acetonitrile. This choice aimed to avoid H_2O and achieved a more uniform and consistent coverage after annealing. The properties of the coating material on NCM851005 were investigated, along with its effect on electrochemical performance in LIBs and thiophosphate-based solid-state batteries (SSBs). Additionally, to the authors' knowledge, this is the first report describing the application of a V-based surface coating to a Ni-rich NCM for SSB purposes.

Results and Discussion

The $TBA_3H_3[V_{10}O_{28}]$ (see Figure 1) was synthesized according to the method outlined by Klemperer.[35] Successful synthesis was confirmed by attenuated total reflection-infrared (ATR-IR) spectroscopy and powder X-ray diffraction (XRD), as illustrated in Figures S1 and S2 in the Supporting Information.

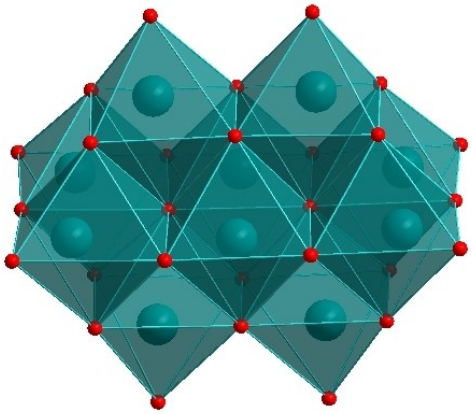

Figure 1. Polyhedral representation of $[V_{10}O_{28}]^{6-}$. Color code: VO_6 octahedra: teal, O: red. The TBA counterion is not shown for clarity.

Thermogravimetric analysis (TGA) was performed to determine the optimal annealing temperature for the V-coated NCM851005. Aside from ensuring close interaction with the CAM particles, the heat treatment is meant to combust the TBA cation, which could induce side reactions during battery operation. The TGA profile (see Figure S3) indicates a mass loss of about 43% between 180 and 300 °C, in accordance with the expected relative weight of the three TBA^+ cations and in line with the literature.[36] Specifically, three annealing temperatures were tested for the coating procedure, namely 300, 400, and 500 °C under O_2 atmosphere, with 500 °C yielding superior electrochemical performance when evaluating the V-coated CAMs in LIB coin cells (3.0–4.3 V vs. Li^+/Li, 25 °C; see Figure S4a). The POV was also tested in different non-aqueous solvents, such as methanol, isopropanol, ethanol, and acetonitrile, with the latter two demonstrating better solubility. The V-coated CAMs prepared using both solvents showed a similar electrochemical performance in terms of long-term stability (see Figure S4b). However, the material prepared in acetonitrile delivered higher specific capacities (by $q_{dis} \approx 10\ mAh\,g^{-1}$), making it the chosen solvent for the following experiments.

To examine the phases formed by the POV upon annealing, the $TBA_3H_3[V_{10}O_{28}]$ precursor was heated at 300 and 500 °C under O_2 atmosphere and probed using XRD. The patterns (see Figure S5) indicate the presence of mainly V_2O_5 and VO_2, with the POV at 500 °C revealing higher intensities for the peaks corresponding to the V_2O_5 phase. Nevertheless, it is important to note that NCM851005 can serve as a source of lithium and induce the formation of other compounds. For instance, ATR-IR analysis of the bare and V-coated samples (see Figure S6) revealed distinct bands corresponding to carbonate species in the spectrum collected from the bare CAM, while the V-coated NCM851005 produced only minor bands in the same region.

The lattice structure of the pristine NCM851005 and the samples with coating contents of 0.5, 1.0, and 3.0 mol.% V (referred to as POV0.5, POV1, and POV3, respectively) was examined by XRD, as shown in Figure 2. The patterns confirm the α-$NaFeO_2$-type structure within the $R-3m$ space group for all samples, as expected for NCMs. As evident from the refined

Research Article
doi.org/10.1002/batt.202400601
Chemistry Europe
European Chemical Societies Publishing

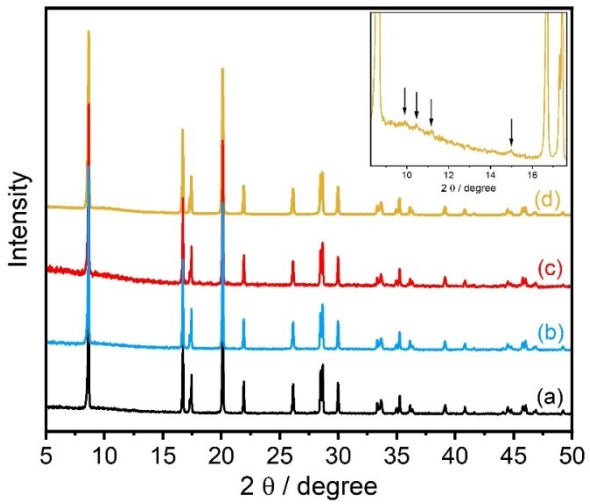

Figure 2. Normalized powder XRD patterns of (a) bare NCM851005, (b) POV0.5, (c) POV1, and (d) POV3. The inset zooms in on the diffractogram of POV3, denoting the peaks corresponding to the Li_3VO_4 phase with arrows.

structural parameters given in Table 1, Rietveld analysis (see example in Figure S7) revealed a minor impact on crystal structure. The slight variations in lattice parameter *c* and unit-cell volume are due to the presence of $Ni_{Li}^{\bullet}$ point defects (Li^{+}/Ni^{2+} mixing), possibly resulting from increasing (bulk) lithium consumption by the V-based coating with increasing coating content. Moreover, reflections related to vanadium compounds were not detected for the POV0.5 and POV1 samples, most likely due to the low coating content. In contrast, POV3, which was also measured for a longer time, exhibited minor reflections between 9 and 20° 2-theta, as indicated in the inset of Figure 2, corresponding to the Li_3VO_4 phase (see also Figure S7). These results suggest that the coating after annealing at 500 °C rather consists of a mixture of phases, namely primarily V_2O_5 and Li_3VO_4.

Scanning electron microscopy (SEM) was employed to examine the morphology and surface characteristics of the POV1 sample. The analysis was conducted after drying the material at 100 °C under vacuum (see Figures 3a–c), followed by annealing at 500 °C (see Figures 3d–f). The expected morphology was observed in either case, with secondary particles of ~4 μm in diameter consisting of primary particles up to several hundred nanometers in size.[37–39] At a higher magnification (see Figures 3c and f), the thin coating on the NCM851005 is more evident. Interestingly, given that POMs commonly serve as building blocks for the formation of nanostructures or films,[40–42] the V-based coating in fact exhibits a film-like appearance. Moreover, the surface coating becomes rougher upon annealing, possibly indicating the conversion of the POV into other V-based materials.

Transmission electron microscopy (TEM) imaging demonstrated the uniformity of coating on the NCM851005 particles, with a thickness ranging from 8 to 28 nm (see Figures 4a–c). At higher magnifications (see Figures 4d–f), lattice fringes were clearly detected, indicative of distinct crystallographic features within the coating. Specifically, the observed *d*-spacing of 4.7 Å corresponds to the layered NCM phase [(003) plane; $R-3m$

Table 1. Rietveld refinement results for the bare and V-coated NCM851005 samples.

Sample	V/Å^3	a/Å	c/Å	$Ni_{Li}^{\bullet}$/%	R_{wp}/%	χ^2
NCM	101.19	2.8700	14.1855	0.7	10.77	0.93
POV0.5	101.22	2.8702	14.1874	1.2	10.86	0.97
POV1	101.19	2.8702	14.1866	1.6	12.07	0.91
POV3	101.30	2.8713	14.1875	3.3	6.21	3.0

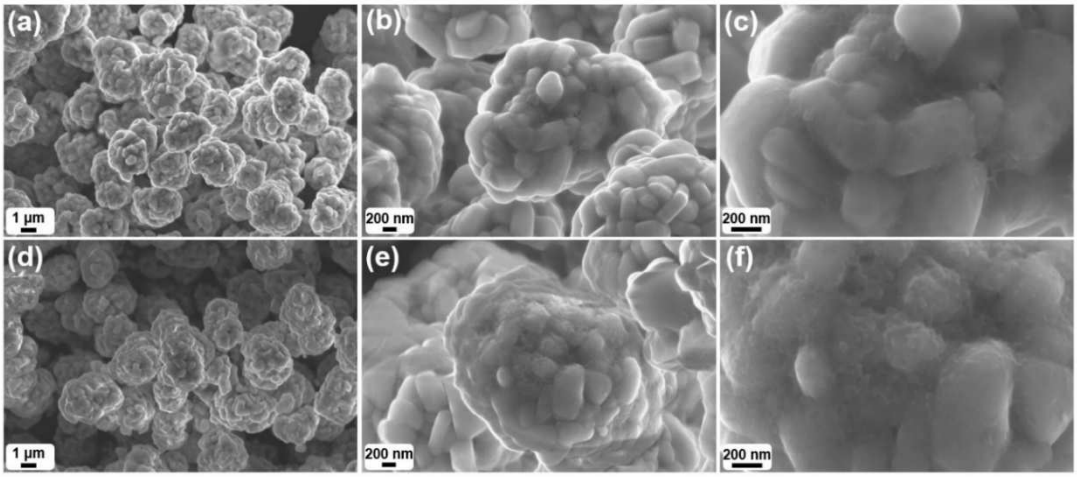

Figure 3. SEM images at different magnifications of POV1 after (a–c) drying at 100 °C and (d–f) heating at 500 °C.

Research Article
doi.org/10.1002/batt.202400601
Chemistry Europe
European Chemical Societies Publishing

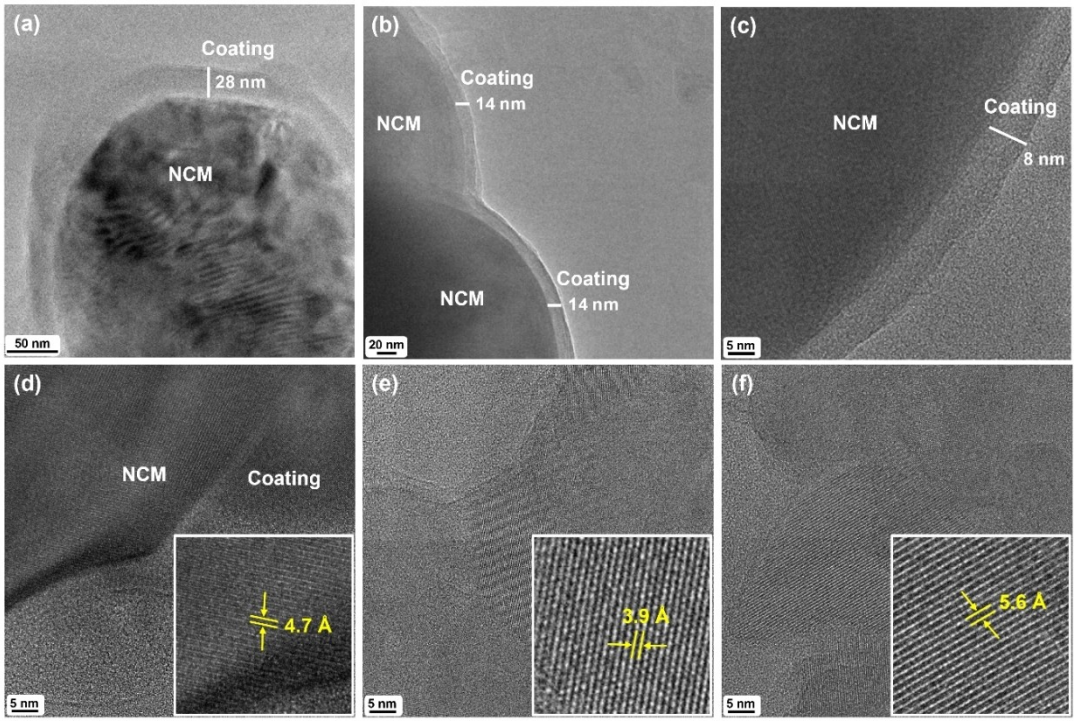

Figure 4. TEM images of POV1 revealing (a–c) thickness and (d–f) composition of the V-based coating.

space group),[43] while the 3.9 and 5.6 Å *d*-spacings are attributed to the (011) plane of Li_3VO_4[44] and the (200) plane of V_2O_5,[45] respectively. These findings agree with the XRD results, confirming Li_3VO_4 and V_2O_5 as components of the surface coating.

Scanning TEM (STEM) images and corresponding elemental maps (see Figures 5a–d and S8a–d) further highlight the coating on the outer surface of a focused ion beam (FIB)-prepared POV1 particle cross section. As can be seen, vanadium is distributed over the whole particle surface, while its diffusion into the bulk was not detected. The carbon likely originates from the Pt deposition, leaving behind residual species on the surface during sample preparation.

The electrochemical behavior of the bare NCM851005 and POV1 CAMs was tested in LIB coin cells with a Li metal anode (3.0–4.3 V vs. Li^+/Li, 25 °C; see Figures 6a–c). Additionally, samples with varying coating contents were evaluated, and the one having 1 mol.% V exhibited the best cycling performance (see Figure S9). The first-cycle charge/discharge curves at a rate of 0.1 C, as shown in Figure 6a, were similar, indicating that the surface coating does not strongly affect the pristine material. Nevertheless, the POV1 cathode delivered a lower initial specific

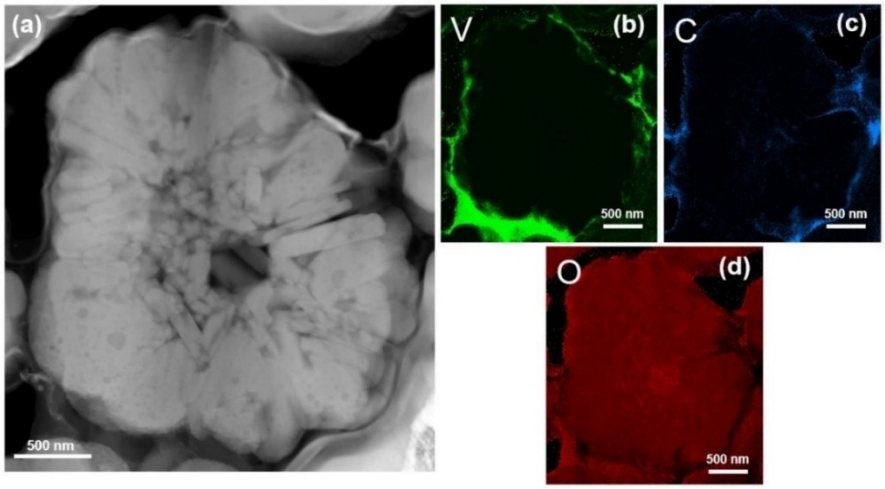

Figure 5. (a) STEM image of POV1 and corresponding elemental mapping of (b) V, (c) C, and (d) O.

Research Article
doi.org/10.1002/batt.202400601
Chemistry Europe
European Chemical Societies Publishing

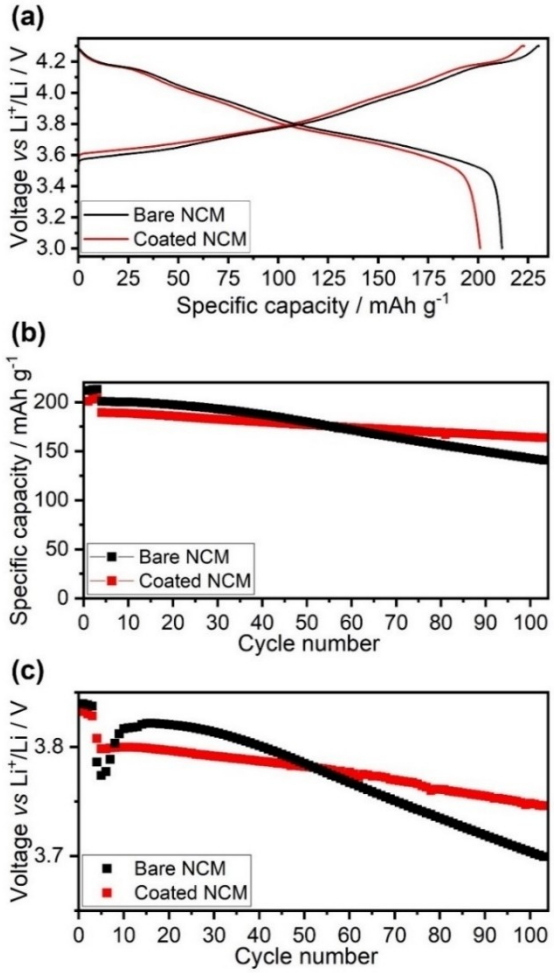

Figure 6. Electrochemical performance of the bare NCM851005 and POV1 in LIB coin cells at 25 °C in a potential range of 3.0–4.3 V vs. Li^+/Li. (a) First-cycle voltage profiles at 0.1 C, (b) specific discharge capacity versus the cycle number, with the first three cycles performed at 0.1 C and the subsequent ones at 0.5 C, and (c) corresponding evolution of mean voltage.

discharge capacity of 201 mAh g^{-1} and Coulomb efficiency of 90 %, compared to 212 mAh g^{-1} and 92 % for the bare NCM851005. Similarly, Liu and coworkers observed reduced initial charge and discharge capacities for NCM111 (2.8–4.5 V vs. Li^+/Li at 300 mA g^{-1}) after coating with 3 wt.% V_2O_5.[46] They attributed this to the coating not contributing to the capacity above 2.8 V, and the absence of V^{4+}/V^{5+} redox under the experimental conditions, as confirmed by cyclic voltammetry (CV) measurements. Regardless, as suggested by XRD, this discrepancy may also be due in part to the consumption of lithium in the formation of Li_3VO_4 and the consequently higher fraction of substitutional ($Ni^{\bullet}_{Li}$) defects (0.7 vs. 1.6 %).

After the first three cycles at 0.1 C, the cells were cycled at 0.5 C for another 100 cycles in the same potential range. The long-term performance of the bare NCM851005 and POV1 cathodes is illustrated in Figure 6b, in which the coated sample provides a much better capacity retention of 87 %, compared to 70 % for the bare NCM851005. In addition, the mean voltage is plotted against the cycle number for both materials in Figure 6c. As can be seen, only the mean voltage of the bare NCM851005 cell varied strongly with changes in C-rate and over cycling, suggesting that the V-based coating effectively mitigates voltage fade during battery operation.

Cross-sectional SEM images comparing the bare NCM851005 and POV1 cathodes (see Figures 7a–f) after cycling further confirm that the coating effectively protects the CAM secondary particles from fracturing and supports their integrity.

Electrochemical impedance spectroscopy (EIS) measurements were also conducted on the bare NCM851005 and POV1 cells after long-term cycling (see Figures 8a and b). One or two semicircles can be identified from the Nyquist plots in the medium-to-low frequency range. In general, the bare CAM showed a much larger resistance than its coated counterpart. To quantitatively analyze the polarization resistance, equivalent circuit model (ECM) fitting was performed, as shown in Figure 8a. The fitted parameters are given in Table S1. R_{bulk} represents the bulk resistance and includes the liquid electro-

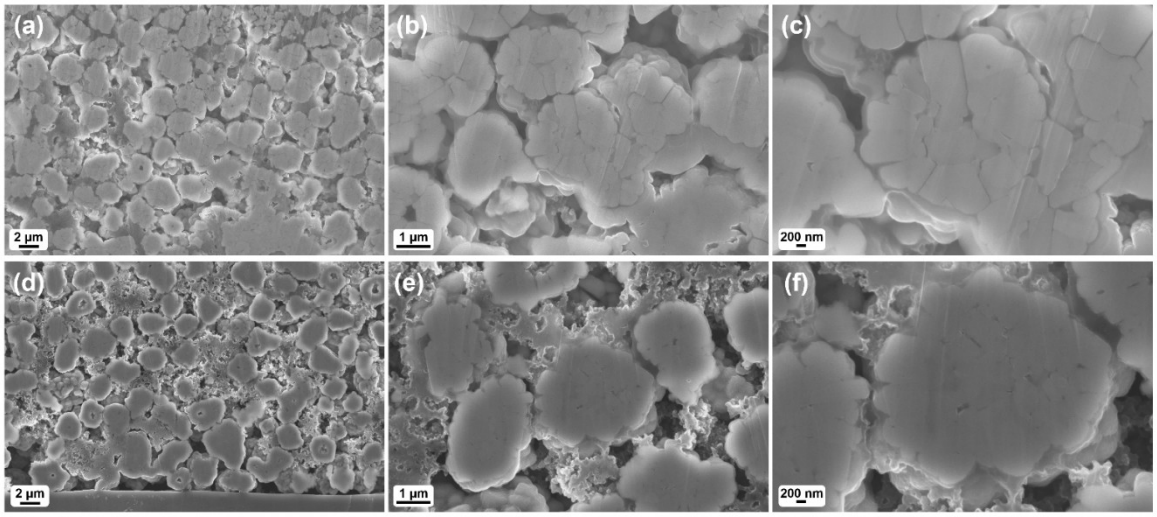

Figure 7. Cross-sectional SEM images of cathodes using (a–c) bare NCM851005 and (d–f) POV1 after 100 cycles at 1 C in LIB coin cells.

Research Article
doi.org/10.1002/batt.202400601
Chemistry Europe
European Chemical Societies Publishing

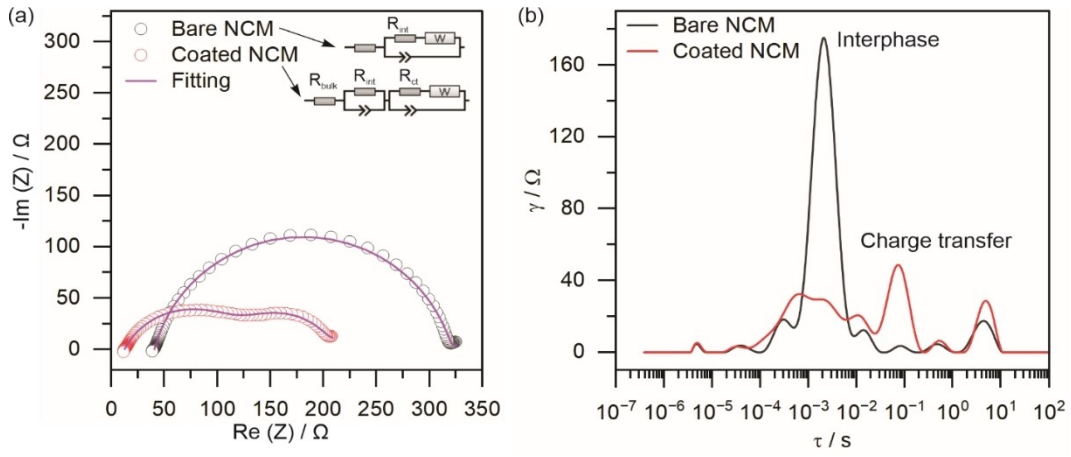

Figure 8. EIS measurements conducted on LIB coin cells at the end of charge after 100 cycles at 1 C. (a) Nyquist plots and ECM fitting for the bare NCM851005 and POV1 and (b) corresponding DRT patterns.

lyte, device connection, and contact resistances between the particles or the electrode and the current collector. The *ZARC* element (resistor, *R*, and constant phase element, *Q*, in parallel) was introduced to represent interface-related kinetic processes, including interphase formation (R_{int}) and charge transfer (R_{ct}). A Warburg element (*W*) was used to fit the semi-infinite diffusion process of the cathodes.

Moreover, to better understand the kinetic processes, corresponding distribution of relaxation times (DRT) analysis was conducted, as shown in Figure 8b. According to the literature,[47] the timescale between 10^{-4} and 10^{-2} s can be attributed to the as-formed interphase(s) at the cathode and anode sides, while the range between 10^{-2} and 10^{0} s reflects major charge-transfer processes at the interfaces. Interestingly, the peak intensity for the (decomposition) interphase(s) was considerably lower for the V-coated CAM. This indicates that fewer side products are formed on the surface compared to the bare NCM851005, suggesting that the coating is indeed capable of mitigating electrolyte degradation. Also, the charge-transfer response was more pronounced, which may be due to better integrity of the CAM particles. In agreement with the kinetic response from DRT analysis, the sum of the fitted interface-related resistances ($R_{int} + R_{ct} = 193.1\ \Omega$) was much smaller for the POV1 (compared to $R_{int} = 280.2\ \Omega$ for the bare NCM851005), indicating less kinetic hindrance after CAM surface coating.

Figures 9a and b show the results from SSB cell testing using argyrodite Li_6PS_5Cl as solid electrolyte (SE) at 45 °C and in a potential range of 2.28–3.68 V vs. In/InLi (approx. 2.9–4.3 V vs. Li^+/Li). Similar to the LIB data, the cells exhibited a comparable electrochemical behavior in the initial cycle at 0.1 C rate (see Figure 9a). However, POV1 achieved a higher specific discharge capacity of $q_{dis} = 204\ mAh\,g^{-1}$, compared to 189 $mAh\,g^{-1}$ for the bare NCM851005, pointing toward improved kinetics (see also rate performance in Figure 9b) and reversibility after coating. It is noteworthy that V_2O_5 and Li_3VO_4 can function both as ion conductor and as electronic insulator, offering potential advantages in mitigating (electro)chemical degradation, particularly oxidation of the thiophosphate solid electrolyte at the CAM | SE

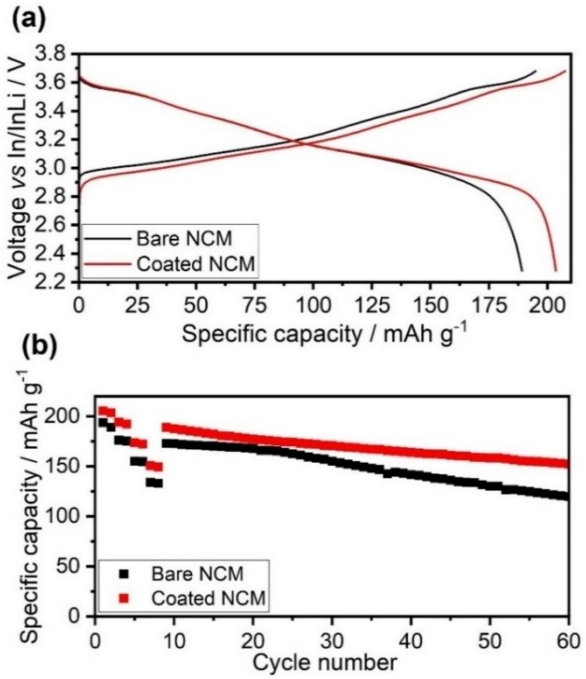

Figure 9. Electrochemical performance of the bare NCM851005 and POV1 in thiophosphate-based SSB cells at 45 °C and in a potential range of 2.28–3.68 V vs. In/InLi. (a) First-cycle voltage profiles at 0.1 C and (b) specific discharge capacity versus the cycle number, with two cycles each at 0.1 C, 0.2 C, 0.5 C, and 1 C, followed by 0.2 C cycling.

interface.[48–50] Therefore, in this case, the beneficial effects from surface coating are already apparent in the initial cycles, unlike in the case of LIBs, where the liquid electrolyte more effectively "interacts" with the CAM particles. After 50 cycles at 0.2 C, the capacity retention was 81 and 69% for the POV1 and bare NCM851005 SSB cells, respectively.

Overall, the findings suggest that the application of coatings derived from POVs or POMs, in general, represents a viable strategy to enhance the cycling performance and stability of Ni-rich NCMs in both LIB and SSB environments.

Conclusions

To enhance the cyclability of Ni-rich NCM cathodes, a coating method was investigated employing the POV, $TBA_3H_3[V_{10}O_{28}]$, chosen for its solubility in non-aqueous solvents. The best electrochemical performance was achieved with the 1 mol.% V coating in acetonitrile and post-annealing at 500 °C under O_2 atmosphere. XRD indicated that the coating consists of a mixture of phases, predominantly V_2O_5 and Li_3VO_4, which was further confirmed by TEM analysis. It exhibits a film-like appearance, with vanadium evenly distributed across the secondary particle surface, while no diffusion into the bulk was observed. Evaluation in LIB cells demonstrated superior capacity retention of 87% for the coated sample after 100 cycles at 0.5 C, compared to 70% for the bare NCM851005. Similarly, in thiophosphate-based SSBs, the capacity retention increased from 69 to 81% (after 50 cycles at 0.2 C).

Taken together, these findings demonstrate the potential of protective coatings derived from POVs as an effective strategy for enhancing the cycling performance and stability of Ni-rich NCMs, offering benefits for both liquid- and solid-state batteries. Future research should focus on optimizing the process and exploring different variants of POVs and other POMs.

Experimental

Coating Procedure

NCM851005 ($d_{50} = 4$ μm) was obtained from BASF SE and further regenerated at 750 °C for 3 h under O_2 atmosphere to remove surface impurities (residual lithium). Appropriate amounts of POV, corresponding to 0.5, 1.0, and 3.0 mol.% of V in relation to NCM851005, were dissolved in 20 mL of acetonitrile. Then, 2 g of CAM was added, and the suspension was sonicated for 30 min. The solvent was removed via rotary evaporation, followed by drying at 100 °C under vacuum. Finally, the V-coated NCM851005 was obtained by annealing at 500 °C (5 °C min^{-1} heating rate) for 2 h in a tube furnace under O_2 atmosphere.

Characterization

Attenuated total reflection-infrared (ATR-IR) spectroscopy of $TBA_3H_3[V_{10}O_{28}]$ was performed using a Nicolet iS50 spectrometer with ATR attachment. For the NCM851005 and POV1 samples, ATR-IR measurements were conducted in an Ar glovebox using an ALPHA FT-IR spectrometer (Bruker).

Powder X-ray diffraction (XRD) of $TBA_3H_3[V_{10}O_{28}]$ was performed on a STOE STADI–P equipped with a Cu-K_α source of characteristic wavelength $\lambda = 1.5405$ Å. Patterns were also collected from the bare NCM851005, POV0.5, POV1, and POV3 samples placed in 0.03 mm glass capillaries (Hilgenberg) using a STADI–P (STOE) diffractometer in Debye-Scherrer geometry. Monochromatic Mo-$K_{\alpha1}$ radiation ($\lambda = 0.7093$ Å, 50 kV, 40 mA) and a Mythen 1 K detector (Dectris) were employed for the measurements. Rietveld refinement was carried out using GSAS-II,[51] allowing variations in scale factor, zero shift, and size/strain broadening parameters. A fixed background was fitted to the data using a 12-term Chebyshev polynomial function. In the structural model, the unit-cell parameters, oxygen *z*-coordinate, and isotropic atomic displacement parameters for each site were refined.

Scanning electron microscopy (SEM) measurements were performed using a LEO-1530 microscope from Carl Zeiss AG equipped with a field emission source. For cross-sectional imaging, an IB-19510CP cross-section polisher (JEOL) with Ar-gas source was used to polish the electrodes.

(Scanning) transmission electron microscopy [(S)TEM] measurements were conducted on a probe-corrected Titan Themis (Thermo Fisher Scientific) at an accelerating voltage of 300 kV. The microscope was equipped with a Super-X detector for energy dispersive X-ray spectroscopy (EDS).

Electrochemical impedance spectroscopy (EIS) measurements were performed on a BioLogic SP-300 potentiostat after long-term cycling with an additional charge at 0.1 C rate and 1 h rest, in a frequency range between 1 MHz and 100 mHz and voltage perturbation of 7 mV. Distribution of relaxation times (DRT) analysis was conducted using the RelaxIS software applying a value of 10^{-5} for the regularization parameter.

Electrochemical Testing

For LIBs, a slurry was prepared combining the CAM with Super C65 carbon additive and polyvinylidene difluoride (PVDF, Solef 5130, Solvay) binder in a weight ratio of 94:3:3. The mixture was cast onto 0.03 mm aluminum foil using a stainless steel doctor blade of slit thickness 140 μm employing an Erichsen Coatmaster 510 film applicator. Subsequently, the cathode tapes were dried at 120 °C overnight under vacuum, calendered at 14 N mm^{-1} (Sumet Messtechnik), and cut into circular 13 mm diameter discs. The areal loading was about 9 mg_{CAM} cm^{-2}. Coin cells were assembled from the prepared cathodes, a Whatman GF/D glass fiber separator, a Li metal anode, and LP57 electrolyte (1 M $LiPF_6$ in a 3:7 weight mixture of ethylene carbonate and ethyl methyl carbonate) in an Ar glovebox. They were crimped under a pressure of 1 t.

For SSBs, cells were assembled following a procedure reported previously.[52] A composite consisting of 69 wt.% CAM, 1 wt.% Super C65, and 30 wt.% Li_6PS_5Cl was prepared by ball milling at 140 rpm for 30 min (of note, 12 mg were used for the cathode preparation). For the separator, 100 mg of Li_6PS_5Cl was used. In/InLi alloy was applied as anode and prepared *in situ* by pressing In and Li foils together. The areal loading was about 11 mg_{CAM} cm^{-2}. The cells were kept at a uniaxial pressure of 81 MPa, and they were cycled in constant current mode at 45 °C. The initial rate test involved two cycles each at 0.1 C, 0.2 C, 0.5 C, and 1 C, followed by 50 cycles at 0.2 C (with 1 C = 190 mA g^{-1}).

Acknowledgements

This work was supported by BASF SE. The authors acknowledge the support from the programmorientierten Förderung (PoF IV) and Karlsruhe Nano Micro Facility (KNMFi, www.knmf.kit.edu), a Helmholtz research infrastructure at Karlsruhe Institute of Technology (KIT, www.kit.edu). B.N.N. is grateful to the Federal Ministry of Education and Research (Bundesministerium für Bildung und Forschung, BMBF) for funding within the project SUSTRAB (03XP0415D). The authors also thank Martin Velazquez-Rizo (KIT) and Rajib Sahu (KIT) for conducting the TEM analysis and Triantafillia Malliaridou for assistance in the laboratory. Open Access funding enabled and organized by Projekt DEAL.

Conflict of Interests

The authors declare no conflict of interest.

Data Availability Statement

The data that support the findings of this study are available from the corresponding author upon reasonable request.

Keywords: Polyoxometalates · Ni-rich NCM · Protective coating · Interfaces · Electro-chemo-mechanical degradation

[1] M. S. Whittingham, *Chem. Rev.* **2004**, *104*, 4271–4302.
[2] Y. Kim, W. M. Seong, A. Manthiram, *Energy Storage Mater.* **2021**, *34*, 250–259.
[3] Z. Ye, L. Qiu, W. Yang, Z. Wu, Y. Liu, G. Wang, Y. Song, B. Zhong, X. Guo, *Chem. Eur. J.* **2021**, *27*, 4249–4269.
[4] M. Bianchini, M. Roca-Ayats, P. Hartmann, T. Brezesinski, J. Janek, *Angew. Chem., Int. Ed.* **2019**, *58*, 10434–10458.
[5] L. de Biasi, B. Schwarz, T. Brezesinski, P. Hartmann, J. Janek, H. Ehrenberg, *Adv. Mater.* **2019**, *31*, 1900985.
[6] Z. Chen, D. Chao, J. Lin, Z. Shen, *Mater. Res. Bull.* **2017**, *96*, 491–502.
[7] D. Weber, Đ. Tripković, K. Kretschmer, M. Bianchini, T. Brezesinski, *Eur. J. Inorg. Chem.* **2020**, *2020*, 3117–3130.
[8] L. Liang, W. Zhang, F. Zhao, D. K. Denis, F. U. Zaman, L. Hou, C. Yuan, *Adv. Mater. Interfaces* **2020**, *7*, 1901749.
[9] N. A. Chernova, M. Roppolo, A. C. Dillon, M. S. Whittingham, *J. Mater. Chem.* **2009**, *19*, 2526–2552.
[10] Y. Yue, H. Liang, *Adv. Energy Mater.* **2017**, *7*, 1602545.
[11] F. Lv, H. Cheng, W. Nie, Q. Sun, Y. Liu, T. Duan, Q. Xu, X. Lu, *ChemistrySelect* **2021**, *6*, 6339–6347.
[12] M. Yuan, Y. Li, Q. Chen, C. Chen, X. Liu, W. Zeng, R. Wang, S. Xiao, *Electrochim. Acta* **2019**, *323*, 134822.
[13] X. Liu, P. He, H. Li, M. Ishida, H. Zhou, *J. Alloys Compd.* **2013**, *552*, 76–82.
[14] Z. Chen, Z. Wang, G.-T. Kim, G. Yang, H. Wang, X. Wang, Y. Huang, S. Passerini, Z. Shen, *ACS Appl. Mater. Interfaces* **2019**, *11*, 26994–27003.
[15] X. Xiong, Z. Wang, H. Guo, Q. Zhang, X. Li, *J. Mater. Chem. A* **2013**, *1*, 1284–1288.
[16] X. Xiong, Z. Wang, G. Yan, H. Guo, X. Li, *J. Power Sources* **2014**, *245*, 183–193.
[17] Y. Lu, X. Zeng, J. Wang, L. Yang, S. Hu, C. Jia, H. Zhao, D. Yin, X. Ge, X. Xi, *Adv. Mater. Interfaces* **2019**, *6*, 1901368.
[18] F. Schipper, E. M. Erickson, C. Erk, J.-Y. Shin, F. F. Chesneau, D. Aurbach, *J. Electrochem. Soc.* **2017**, *164*, A6220–A6228.
[19] D. Pritzl, T. Teufl, A. T. S. Freiberg, B. Strehle, J. Sicklinger, H. Sommer, P. Hartmann, H. A. Gasteiger, *J. Electrochem. Soc.* **2019**, *166*, A4056–A4066.
[20] J. Sicklinger, M. Metzger, H. Beyer, D. Pritzl, H. A. Gasteiger, *J. Electrochem. Soc.* **2019**, *166*, A2322–A2335.
[21] D.-H. Cho, C.-H. Jo, W. Cho, Y.-J. Kim, H. Yashiro, Y.-K. Sun, S.-T. Myung, *J. Electrochem. Soc.* **2014**, *161*, A920–A926.
[22] G. V. Zhuang, G. Chen, J. Shim, X. Song, P. N. Ross, T. J. Richardson, *J. Power Sources* **2004**, *134*, 293–297.
[23] B. Zhang, P. Dong, H. Tong, Y. Yao, J. Zheng, W. Yu, J. Zhang, D. Chu, *J. Alloys Compd.* **2017**, *706*, 198–204.
[24] W. Wang, Z. Yin, Z. Wang, X. Li, H. Guo, *Mater. Lett.* **2015**, *160*, 298–301.
[25] Y. Huang, F.-M. Jin, F.-J. Chen, L. Chen, *J. Power Sources* **2014**, *256*, 1–7.
[26] Y.-F. Song, R. Tsunashima, *Chem. Soc. Rev.* **2012**, *41*, 7384–7402.
[27] D. Long, R. Tsunashima, L. Cronin, *Angew. Chem., Int. Ed.* **2010**, *49*, 1736–1758.
[28] Y. Zhang, J. Liu, S.-L. Li, Z.-M. Su, Y.-Q. Lan, *EnergyChem* **2019**, *1*, 100021.
[29] H. Wang, S. Hamanaka, Y. Nishimoto, S. Irle, T. Yokoyama, H. Yoshikawa, K. Awaga, *J. Am. Chem. Soc.* **2012**, *134*, 4918–4924.
[30] T. Zhou, L.-L. Xie, Y. Niu, H.-R. Xiao, Y.-J. Li, Q. Han, X.-J. Qiu, X.-L. Yang, X.-Y. Wu, L.-M. Zhu, H. Pang, X.-Y. Cao, *Rare Met.* **2023**, *42*, 1431–1445.
[31] M. Anjass, G. A. Lowe, C. Streb, *Angew. Chem., Int. Ed.* **2021**, *60*, 7522–7532.
[32] R. C. McNulty, K. Penston, S. S. Amin, S. Stal, J. Y. Lee, M. Samperi, L. Pérez-García, J. M. Cameron, L. R. Johnson, D. B. Amabilino, G. N. Newton, *Angew. Chem., Int. Ed.* **2023**, *135*, e202216066.
[33] A. Bayaguud, Z. Zhang, M. Geng, Y. Fu, Y. Yu, C. Zhu, *Small Methods* **2019**, *3*, 1900187.
[34] M. H. Anjass, M. Deisböck, S. Greiner, M. Fichtner, C. Streb, *ChemElectroChem* **2019**, *6*, 398–403.
[35] W. G. Klemperer, in *Inorganic Syntheses* (Ed.: A. P. Ginsberg), John Wiley & Sons, **1990**, *27*, pp. 83–85.
[36] M. Ghosh, D. Sorsche, R. Binte Ahmed, M. Anjass, *ChemSusChem* **2023**, *16*, e202300631.
[37] D. Kitsche, Y. Tang, H. Hemmelmann, F. Walther, M. Bianchini, A. Kondrakov, J. Janek, T. Brezesinski, *Small Sci.* **2023**, *3*, 2200073.
[38] S. L. Dreyer, K. R. Kretschmer, Đ. Tripković, A. Mazilkin, R. Chukwu, R. Azmi, P. Hartmann, M. Bianchini, T. Brezesinski, J. Janek, *Adv. Mater. Interfaces* **2022**, *9*, 2101100.
[39] Y. Ma, J. H. Teo, F. Walther, Y. Ma, R. Zhang, A. Mazilkin, Y. Tang, D. Goonetilleke, J. Janek, M. Bianchini, T. Brezesinski, *Adv. Funct. Mater.* **2022**, *32*, 2111829.
[40] S. Liu, D. Volkmer, D. G. Kurth, *J. Clust. Sci.* **2003**, *14*, 405–419.
[41] D.-L. Long, E. Burkholder, L. Cronin, *Chem. Soc. Rev.* **2007**, *36*, 105–121.
[42] W. Yang, L.-H. Gao, K.-Z. Wang, *Polyhedron* **2014**, *82*, 80–87.
[43] M. Ge, S. Wi, X. Liu, J. Bai, S. Ehrlich, D. Lu, W.-K. Lee, Z. Chen, F. Wang, *Angew. Chem., Int. Ed.* **2021**, *60*, 17350–17355.
[44] Z. Chen, Z. Zhang, X. Dong, Y. Shi, Y. Liu, Q. Jing, *Cryst. Growth Des.* **2017**, *17*, 2792–2800.
[45] R. Haberkorn, J. Bauer, G. Kickelbick, *Z. Anorg. Allg. Chem.* **2014**, *640*, 3197–3202.
[46] X. Liu, P. He, H. Li, M. Ishida, H. Zhou, *J. Alloys Compd.* **2013**, *552*, 76–82.
[47] Y. Lu, C.-Z. Zhao, J.-Q. Huang, Q. Zhang, *Joule* **2022**, *6*, 1172–1198.
[48] W.-T. Kim, Y. U. Jeong, Y. J. Lee, Y. J. Kim, J. H. Song, *J. Power Sources* **2013**, *244*, 557–560.
[49] H. Li, X. Liu, T. Zhai, D. Li, H. Zhou, *Adv. Energy Mater.* **2013**, *3*, 428–432.
[50] Y. Wang, K. Takahashi, K. H. Lee, G. Z. Cao, *Adv. Funct. Mater.* **2006**, *16*, 1133–1144.
[51] B. H. Toby, R. B. Von Dreele, *J. Appl. Crystallogr.* **2013**, *46*, 544–549.
[52] D. Kitsche, F. Strauss, Y. Tang, N. Bartnick, A-Y. Kim, Y. Ma, C. Kübel, J. Janek, T. Brezesinski, *Batter. Supercaps* **2022**, *5*, e202100397.

Manuscript received: September 12, 2024
Revised manuscript received: November 5, 2024
Accepted manuscript online: November 6, 2024
Version of record online: November 20, 2024